Evaluation of an urban canopy model in a tropical city: the role of tree evapotranspiration

Environmental Research Letters

LETTER

Evaluation of an urban canopy model in a tropical city: the role of tree evapotranspiration

Xuan Liu[1], Xian-Xiang Li[1,3], Suraj Harshan[2], Matthias Roth[2] and Erik Velasco[1]

[1] CENSAM, Singapore-MIT Alliance for Research and Technology, Singapore
[2] Department of Geography, National University of Singapore, Singapore
[3] Author to whom any correspondence should be addressed.

E-mail: lixx@smart.mit.edu

Keywords: energy balance, hydrological, urban canopy model, tropical, tree evapotranspiration

Supplementary material for this article is available online

OPEN ACCESS

RECEIVED
6 April 2017

REVISED
26 June 2017

ACCEPTED FOR PUBLICATION
11 July 2017

PUBLISHED
11 September 2017

Abstract

A single layer urban canopy model (SLUCM) with enhanced hydrologic processes, is evaluated in a tropical city, Singapore. The evaluation was performed using an 11 month offline simulation with the coupled Noah land surface model/SLUCM over a compact low-rise residential area. Various hydrological processes are considered, including anthropogenic latent heat release, and evaporation from impervious urban facets. Results show that the prediction of energy fluxes, in particular latent heat flux, is improved when these processes were included. However, the simulated latent heat flux is still underestimated by ~40%. Considering Singapore's high green cover ratio, the tree evapotranspiration process is introduced into the model, which significantly improves the simulated latent heat flux. In particular, the systematic error of the model is greatly reduced, and becomes lower than the unsystematic error in some seasons. The effect of tree evapotranspiration on the urban surface energy balance is further demonstrated during an unusual dry spell. The present study demonstrates that even at sites with relatively low (11%) tree coverage, ignoring evapotranspiration from trees may cause serious underestimation of the latent heat flux and atmospheric humidity. The improved model is also transferable to other tropical or temperate regions to study the impact of tree evapotranspiration on urban climate.

1. Introduction

Due to the accelerated worldwide urbanization since the late 20th century, large expanses of natural surfaces have been converted to urban landscapes with implications for albedo (usually lower), surface roughness (higher), evaporation (less), transpiration (less), heat storage capacity (higher) and anthropogenic heat emissions (higher). These changes of underlying surface properties have led to more complex surface energy distribution in urban areas. In addition to impacting the local and regional climate (Grimm *et al* 2008), they may further bring adverse effects to human health (Patz *et al* 2005).

The urban canopy layer (UCL) is the layer between the surface and the mean height of buildings and trees. Its characteristics are dominated by the energy and mass exchange between individual surface facets and the canyon air (Oke 1976). With the recognition of the important roles played by urban areas in surface energy balance (SEB), various numerical models have been developed to investigate the energy exchange over cities, as well as the transfer of momentum and moisture between UCL and the overlying atmosphere. One type of such models is the physically based urban canopy models (UCMs), which explicitly consider the impacts of urban building morphology when calculating the SEB. The UCMs can be further categorized into two types (Fernando 2012): single-layer (Kusaka *et al* 2001) and multilayer (Martilli 2002) schemes. The single-layer urban canopy model (SLUCM) simply represents the urban geometry as two-dimensional street canyons with infinite length but considers the three-dimensional nature of urban morphologies, the shadowing from buildings, and reflection of radiation in the canopy layer. These models calculate the prognostic variables such as surface skin temperature and heat fluxes produced from urban facets (i.e.

building roofs, walls and roads). Chen *et al* (2004) and Miao *et al* (2009) have coupled SLUCM into mesoscale atmospheric models (e.g. Weather Research and Forecasting, WRF model) to offer feasible lower boundary conditions to the overlying atmosphere. The coupled WRF/SLUCM system has been successfully applied in various cities around the world (Chen *et al* 2011) for studying various microclimatic phenomena such as the urban heat island effect (e.g. Miao *et al* 2009, Li *et al* 2013, Li *et al* 2016).

The SLUCM has achieved satisfactory performance in predicting net radiation and sensible heat flux but is still inadequate in predicting latent heat flux (e.g. Loridan *et al* 2010, Li *et al* 2013). Comparing 33 urban SEB models, Grimmond *et al* (2011) concluded that the underestimation of latent heat flux exists not only in SLUCM but also in most other urban land surface schemes. This mainly results from the uncertain mechanism of complex water vapor transport and the inadequate representation of urban hydrological processes, urban vegetation and soil properties. The underestimation of latent heat flux usually leads to overestimation of sensible heat flux and surface skin temperature, which ultimately jeopardizes the SLUCM's accuracy. In order to improve the simulation accuracy of latent heat flux, Loridan *et al* (2010) assessed the fitness of a coupled Noah land surface model/SLUCM parameterization scheme and suggested that a vegetation class like 'cropland/grassland mosaic' or 'grassland' with a low stomatal resistance could help improve the insufficient representation of urban evaporation in the SLUCM. Miao and Chen (2014) and Yang *et al* (2015) included several additional urban hydrological processes (i.e. the anthropogenic latent heat, urban irrigation, evaporation from paved surfaces, and the urban oasis effect) in the coupled Noah/SLUCM to enhance the urban evaporation components. Their evaluation of the model performance in Beijing, Phoenix, Vancouver and Montreal showed that the latent heat flux simulated by the new model improved substantially.

The latent heat flux is especially important since it impacts soil moisture dynamics, surface runoff, and the overlying atmosphere (Koster 2015). Accurate information about the latent heat flux and evapotranspiration is essential for estimating urban ecosystem water requirements and stress regimes, which is of utmost importance during a drought. However, urban latent heat flux and evapotranspiration measurement and estimates are sparse in both time and space (Gentine *et al* 2016). Accurate prediction of latent heat flux will therefore widely benefit the scientific community, urban designers and policy-makers (e.g. Mitchell *et al* 2008). It has been demonstrated that including vegetation effects in urban SEB models is crucial to obtain accurate prediction of the sensible and latent heat fluxes (Best and Grimmond 2015, 2016). In previous urban SEB models, the urban vegetation was usually represented by 'grassland' and the impact of urban trees was neglected in UCMs. Lee and Park (2008) included trees in their SLUCM but did not consider sub-surface moisture transport. Krayenhoff *et al* (2014, 2015) incorporated trees into a multilayer UCM and added tree-building interaction, but they did not fully take the evaporative impact of trees into account. Ryu *et al* (2016) included the hydrothermal processes associated with trees in SLUCM and adequately incorporated the interaction of trees, ground and walls. Their simulation results in three urban/suburban sites in Basel, Switzerland showed improved prediction performance of latent heat flux. The abovementioned models with tree effects revealed the important role of urban trees in SEB modeling, especially in simulating latent heat flux.

In the light of previous studies and the need of accurate prediction of latent heat flux for urban climate modeling, we will conduct an evaluation study in a tropical city Singapore using the coupled Noah/SLUCM model with physically-based urban hydrological processes and tree evapotranspiration. Some previous evaluation studies have been carried out in Singapore (Harshan *et al* 2017, Demuzere *et al* 2017), but neither evaluated the role of tree evapotranspiration. The aims of our study are: (1) evaluate the performance of Noah/SLUCM in a tropical residential neighborhood; (2) improve the capability of this model with urban hydrological processes and tree evapotranspiration; and (3) assess the importance of urban trees in the urban SEB in Singapore.

2. Methods

2.1. Local climate and data collection

Singapore is a tropical city state located at the southern tip of the Malay Peninsula. It is a highly urbanized coastal city with a very high population density of 7821 persons per km^2. As a 'City in the Garden', about half of its land is covered by managed vegetation and young secondary forest (Yee *et al* 2011). Because of its geographical location near the equator, Singapore has a typical equatorial wet climate characterized by perennial high temperature, high humidity and abundant precipitation. Alternating northeast and southwest monsoon winds blowing throughout the island divides its annual climate into a northeast monsoon season (usually December to early March of the following year), a southwest monsoon season (usually June to September) and two inter-monsoon periods (Fong and Ng 2012).

A 23.7 m high eddy-covariance (EC) flux tower is located in Telok Kurau (1°18′51.46″N, 103°54′40.31″E, elevation: ~10 m a.s.l), a low-density residential area in Southeast Singapore. The study area corresponds to 'compact low-rise' or Local Climate Zone 3 according to Stewart and Oke (2012). Given a mean building height of 9.86 m, the sensors are expected to be located with the inertial sublayer (above 2–5 times the height of the

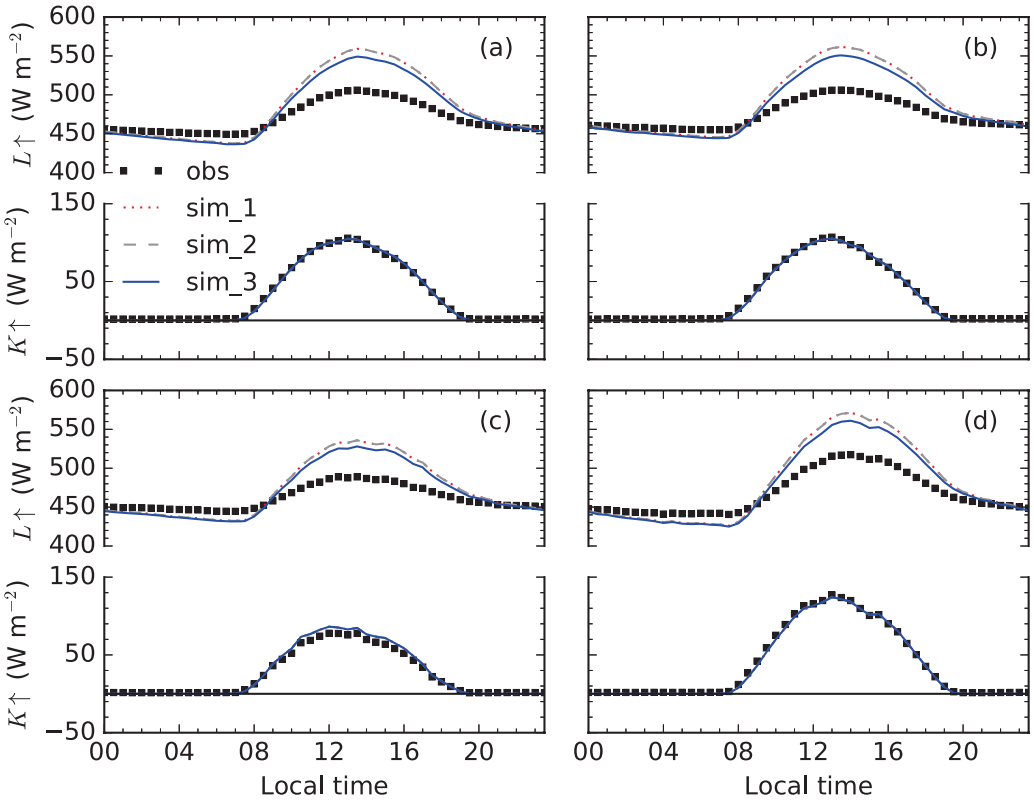

Figure 1. Averaged diurnal profiles of observed (symbols) and simulated (lines) $L_\uparrow$ and $K_\uparrow$ for the (*a*) entire period, (*b*) SW monsoon, (*c*) early NE monsoon, and (*d*) dry period. The definitions of different seasons are detailed in table 3.

surface roughness according to Roth 2000) where fluxes are constant with height and representative of the underlying surface. Within a 1 km radius of the tower, 39% of the plan area is covered by mainly 2–3 story high residential buildings, 12% roads, 34% other impervious surfaces and 15% vegetation (including 11% tree crowns and 4% grassland) with little directional variation (figure S1 in Velasco *et al* 2013). Average flux footprints, which encompass the area on the ground which contributes to the measurement, extended to between 400 m (daytime) to 1000 m (nighttime) from the tower (figure S7 in Velasco *et al* 2013, figure 1 in Roth *et al* 2017). Under most atmospheric conditions the measured fluxes therefore represent the local area of interest. Individual variables were sampled at 10 Hz by EC sensors installed at the top of the tower. Fluxes were calculated for 30 min periods following standard correction and data quality assurance. A detailed description of the instrumentation and flux post-processing are provided in Velasco *et al* (2013) and Roth *et al* (2017). The dataset used in the present study was gap-filled (Harshan *et al* 2017) and used in other studies to evaluate urban land surface models (LSM) to predict SEB fluxes (Harshan *et al* 2017, Demuzere *et al* 2017).

2.2. Coupled Noah/SLUCM model

The coupled Noah/SLUCM is utilized in this study. The heat fluxes associated with the different urban facets (building roofs and walls, roads and other impervious surfaces) are simulated by SLUCM, while those from the vegetation fraction are handled by the Noah LSM (Chen and Dudhia 2001). The urban SEB equations are (Oke 1988)

$$Q^* = K_\downarrow - K_\uparrow + L_\downarrow - L_\uparrow, \quad (1)$$

$$Q^* + Q_F = Q_H + Q_E + \Delta Q_S, \quad (2)$$

where $K_\uparrow$ and $K_\downarrow$ are upwelling and downwelling shortwave radiation, $L_\uparrow$ and $L_\downarrow$ are upwelling and downwelling longwave radiation; Q^* is net radiation, Q_F is anthropogenic heat flux, Q_H is sensible heat flux, Q_E is latent heat flux and Q_S is heat storage. More details of the coupled Noah/SLUCM model can be found in Chen *et al* (2011).

This coupled Noah/SLUCM model was run off-line driven by the 30 minute meteorological and radiation data collected from the EC flux tower, including wind speed, air temperature, relative humidity, ambient pressure, precipitation, downward shortwave and longwave radiation. Other input parameters of urban geometry, building materials and anthropogenic heat used in this study are given in table 1.

2.3. Enhanced hydrological processes

In order to mitigate the deficiency in modeling the latent heat flux in urban LSM models, Miao and Chen (2014) and Yang *et al* (2015) proposed to include some enhanced hydrological processes in the coupled Noah/SLUCM model. These processes are (1) anthropogenic heat flux release, (2) the urban oasis

Table 1. Input parameters for the coupled Noah/SLUCM model in this study.

Input parameters	Units	Value	Reference
Urban category	—	Low-density residential	(Roth *et al* 2017)
Impervious fraction	%	85	(Velasco *et al* 2013)
Tree fraction	%	11	(Velasco *et al* 2013)
Building height	m	9.86	(Velasco *et al* 2013)
Tree height	m	7.26	(Velasco *et al* 2013)
Maximum anthropogenic heat Q_{AHMAX}[a]	W m^{-2}	13	(Quah and Roth 2012)
Roof albedo	—	0.20	(Li *et al* 2013)
Wall albedo	—	0.10	(Li *et al* 2013)
Road albedo	—	0.10	(Li *et al* 2013)
Road width	m	5	(Li *et al* 2013)
Leaf area index of tree	—	3	(Tan and Sia 2010)

[a] Estimated using a combination of top-down and bottom-up modelling approaches of energy consumption applied to the study area.

effect (a phenomenon that patchy vegetation in urban areas has higher rates of potential evapotranspiration than large area vegetation in the natural environment, Hagishima *et al* 2007), (3) urban irrigation and (4) a modified evaporation scheme over urban impervious surfaces. Because the oasis effect is location specific and there is no routine urban irrigation in Singapore, these two processes are not considered in the present study. Instead, a sensitivity study of the oasis effect will be conducted in the supplementary material (section S3 available at stacks.iop.org/ERL/12/094008/mmedia). Considering the other hydrological processes, the latent heat flux can be calculated from two combined sources, urban and non-urban, according to Yang *et al* (2015), as

$$Q_{\mathrm{E}} = f_{\mathrm{urb}}(Q_{\mathrm{Eurb}} + Q_{\mathrm{ALH}}) + f_{\mathrm{veg}} Q_{\mathrm{Eveg}}, \quad (3)$$

$$Q_{\mathrm{Eveg}} = C_H E_p, \quad (4)$$

where f_{urb} is the urban (impervious) fraction, f_{veg} is the vegetation fraction, Q_{Eurb} is the latent heat flux from the urban sources calculated by the original SLUCM, Q_{Eveg} is the latent heat flux produced by non-urban sources. C_{H} is the exchange coefficient, E_p is the potential evaporation rate, Q_{ALH} is anthropogenic latent heat flux, which is calculated as (Yang *et al* 2015)

$$Q_{\mathrm{ALH}} = Q_{\mathrm{ALHMAX}} f_{\mathrm{ALH}}, \quad (5)$$

$$\frac{Q_{\mathrm{ALHMAX}}}{Q_{\mathrm{ASHMAX}}} = \beta \frac{\Delta}{\gamma}, \quad (6)$$

$$Q_{\mathrm{ALHMAX}} + Q_{\mathrm{ASHMAX}} = Q_{\mathrm{AHMAX}}, \quad (7)$$

where Δ is the slope of the saturation vapor pressure curve (kPa K^{-1}), γ is the psychrometric constant (66.1 Pa K^{-1}), β is the moisture availability parameter (a value of 1.5 is used here following Yang *et al* 2015). Q_{ALHMAX}, Q_{ASHMAX} and Q_{AHMAX} are daily maximum anthropogenic latent, sensible and total heat flux, respectively. f_{ALH} is the diurnally-varying coefficient of anthropogenic sensible and latent heat. Q_{AHMAX} and f_{ALH} are both taken from Quah and Roth (2012) and Li *et al* (2013).

Many studies have demonstrated that urban impervious surfaces can partly store precipitation and supply evaporation over a given period of time (e.g. Kawai and Kanda 2010, Ramamurthy and Bou-Zeid 2014). The default evaporation scheme for impervious surfaces only considers the evaporation on the ground surface during precipitation, but excludes water availabilities from ponded surface water due to impeded drainage after precipitation. Based on the hypothesis that water availabilities in road, roof and wall exponentially decrease to 0 in 24 h since last precipitation, Miao and Chen (2014) proposed a new evaporation scheme over urban impervious surfaces in calculating Q_{Eurb} (referred to as the new impervious evaporation scheme hereafter). It is noteworthy that this new impervious evaporation scheme is only applicable in the cases of consecutive precipitation and poor drainage, and therefore in this study we only apply it during the early NE monsoon season.

2.4. Tree evapotranspiration

To account for the tree evapotranspiration effect, a new term is added to equation (3):

$$Q_{\mathrm{E}} = f_{\mathrm{urb}}(Q_{\mathrm{Eurb}} + Q_{\mathrm{ALH}}) + f_{\mathrm{veg}} Q_{\mathrm{Eveg}} + f_{\mathrm{tree}} Q_{\mathrm{Etree}}, \quad (8)$$

where f_{tree} is the tree fraction and Q_{Etree} is the latent heat flux produced by trees, which is calculated using the Penman–Monteith equation (Bosveld and Bouten 2001, Ballinas and Barradas 2016)

$$Q_{\mathrm{Etree}} = \lambda_{\mathrm{v}} ET = \frac{\Delta Q^* + \rho C_P \left(\frac{VPD}{r_{\mathrm{A}}}\right)}{\Delta + \gamma\left(1 + \frac{r_{\mathrm{C}}}{r_{\mathrm{A}}}\right)}, \quad (9)$$

where λ_{v} is latent heat of vaporization of water (J kg^{-1}), ET is the mass water evapotranspiration

Table 2. Designs of numerical simulations to evaluate the importance of hydrological processes and tree evapotranspiration.

Simulation	Enhanced hydrological process		Tree evapotranspiration
	Anthropogenic latent heat	Evaporation on impervious surfaces	
Sim_1	No	Default scheme	No
Sim_2	Yes	The new impervious evaporation scheme for early NE monsoon season	No
Sim_3	Yes	The new impervious evaporation scheme for early NE monsoon season	Yes

Table 3. Seasonal division for the study period.

Code	Period	Number of days	Description
Entire period	18 May 2013–19 Apr 2014	337	
SW monsoon	01 Jun 2013–15 Oct 2013	137	Southwest monsoon
Early NE monsoon	16 Nov 2013–12 Jan 2014	58	Early northeast monsoon
Dry period	13 Jan 2014–15 Mar 2014	62	Prolonged dry spell

rate (kg $s^{-1}m^{-2}$), ρ is the density of air (kg m^{-3}), C_P is the specific heat capacity of air at constant pressure (J $kg^{-1}K^{-1}$), VPD is the vapor pressure deficit (kPa), r_A is the bulk surface aerodynamic resistance for water vapor (s m^{-1}), and r_C is the canopy surface resistance (s m^{-1}). The vapor pressure deficit is calculated by

$$VPD = e_s - e_a = e_s(1 - RH), \qquad (10)$$

where e_s and e_a are saturation vapor pressure (kPa) and vapor pressure (kPa), respectively, and RH is relative humidity. The bulk surface aerodynamic resistance r_A is calculated according to Allen *et al* (1998) as

$$r_A = \frac{1}{k^2 u} \ln\left(\frac{z_m - d}{z_{om}}\right) \ln\left(\frac{z_h - z_d}{z_{oh}}\right), \qquad (11)$$

where k is the von Karman's constant (= 0.41), u is the wind speed at height z_m (m s^{-1}), z_m is the height of wind measurement (m), z_h is the height of humidity measurement (m), z_d is the zero plane displacement height (m), z_{om} is the aerodynamic roughness length for momentum transfer (m) and z_{oh} is the aerodynamic roughness length for the transfer of heat and vapor (m). The zero-plane displacement height z_d is estimated as 0.67 z_r, where z_r is the canopy height (m). In this study, z_{oh} is calculated as 0.1 z_{tree}, where z_{tree} is the mean height of trees (m), while z_{om} is calculated as 0.1 z_{oh}. The canopy surface resistance r_C is calculated following Chen and Dudhia (2001).

2.5. Numerical experiment design

The impact of different processes on the performance of the coupled Noah/SLUCM model was evaluated through three numerical experiments (table 2). Sim_1 used the original model without any additional effects. Sim_2 considered the enhanced hydrological processes including (1) anthropogenic latent heat release, and (2) the evaporation from impervious surfaces (Miao and Chen 2014). Sim_3 further included the tree evapotranspiration in addition to those enhanced hydrological processes considered in Sim_2.

3. Model evaluation

3.1. Study period

The study period spans 11 months from 18 May 2013 to 19 Apr 2014 ('Entire period' hereafter). Considering the climate characteristics of Singapore, two seasons were identified following the monsoon season partitioning in 2013–2014 according to NEA annual weather report (MSS 2014): southwest monsoon season ('SW monsoon' hereafter) and early northeast monsoon season ('Early NE monsoon' hereafter). Detailed seasonal division is shown in table 3. In southwest monsoon season, this island experiences dry wind southerly to southeasterly, resulting in less rainfall comparing to other months of the year. While in the early northeast monsoon season (usually the wettest months within the year), northeast monsoon surges often bring consecutive and widespread heavy rainfalls. Another season is an unusually prolonged dry period ('Dry period' hereafter), during which Singapore suffered the longest dry spell since the beginning of its official records in 1929 (McBride *et al* 2015). During this period, the climate station located at Changi airport only recorded 0.2 mm rainfall, while 2.2 mm rainfall was observed at Telok Kurau. Through conducting the simulations during these seasons which represent Singapore's year-round climate conditions, we attempt to evaluate this coupled Noah/SLUCM model and its modified versions at an equatorial tropical site. In the following sections,

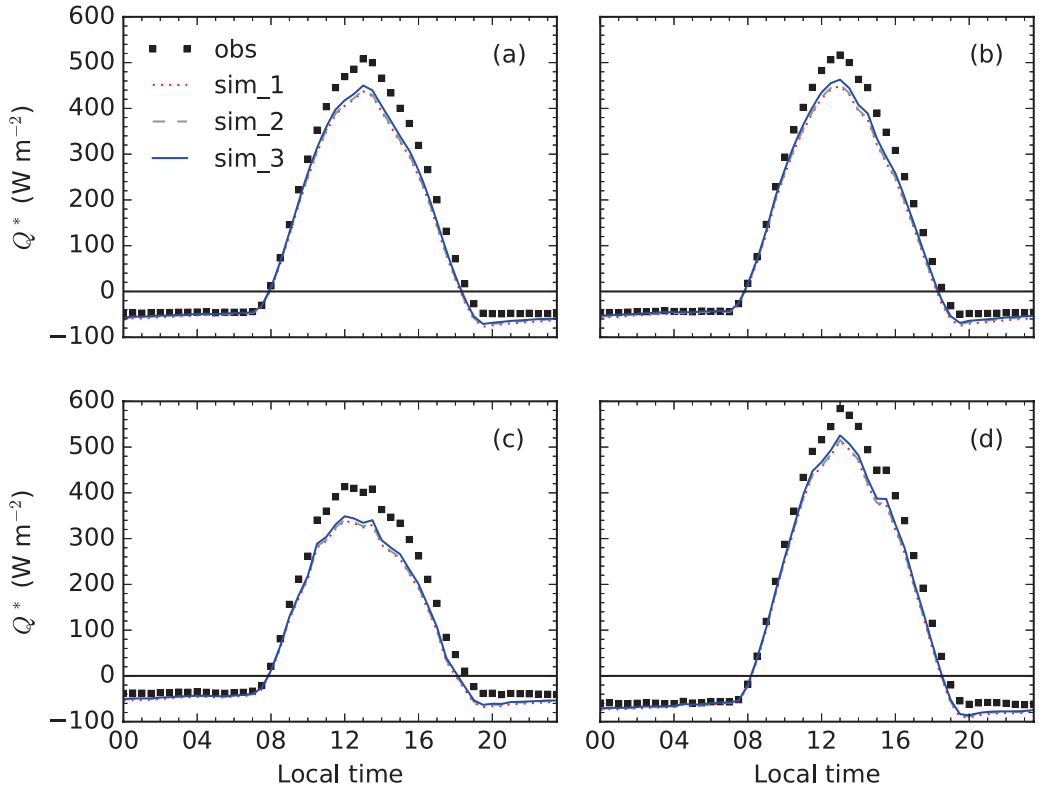

Figure 2. Same as figure 1 but for $Q*$.

the daytime refers to 0800–1800 LT, and nighttime refers to 2000–0600 LT every day.

3.2. Radiation and SEB validation

3.2.1. Upwelling radiation $K_\uparrow$ and $L_\uparrow$

Figure 1 compares the observed and simulated upwelling radiation for each experiment and season. Since the additional processes included in Sim_2 and Sim_3 do not alter the albedo of the underlying surfaces, no variations of the simulated $K_\uparrow$ are observed between the three experiments. In general, the simulated $K_\uparrow$ all agree well with the corresponding observations. Only a slight overestimation in the early NE monsoon season is observed, possibly due to the water accumulation over paved surfaces resulted from consecutive rainfalls in this season. This surface wetness change leads to a lower albedo, while the model albedo keeps constant for all cases.

The simulated $L_\uparrow$ is generally overestimated during daytime (by about 10%) while slightly underestimated just before sunrise (figure 1). It is generally more complex in modeling $L_\uparrow$ than $K_\uparrow$ since $L_\uparrow$ depends strongly on the surface temperature, which in turn is difficult to reproduce given the heterogeneity of materials and geometries within the urban fabric (Grimmond *et al* 2011). In Sim_3, the error of the simulated $L_\uparrow$ during daytime decreases by about 20% compared with the other two experiments, suggesting a better performance after considering tree evapotranspiration effects, although the simulated $L_\uparrow$ is still overestimated during daytime. This suggests that the tree evapotranspiration contributes more to the reduced surface temperature than the other hydrological processes considered.

3.2.2. Net radiation Q^*

The net radiation Q^* is calculated by equation (1), while the downwelling components are from the input forcing data, i.e. the measured data from the EC flux tower. Due to the aforementioned overestimation of $L_\uparrow$, Q^* is always underestimated. The simulation performance of Q^* is generally excellent in terms of the statistic metrics and the performance does not vary much across different seasons (figure 2). The index of agreement (IOA) remains in the interval of 0.97–0.99 during the entire day and during daytime, but decreases slightly during nighttime (table S1). Although the effect is only marginal, the introduction of the hydrological processes and tree evapotranspiration leads to a continuous reduction of root-mean-square error (RMSE), indicating their positive role in improving the simulated Q^*. It is noteworthy that the reduction of the systematic RMSE (RMSEs, table S1) suggests an improvement in the model's prediction skills after considering the tree effect.

3.2.3. Latent heat flux Q_E

Q_E is usually the least well-modelled energy flux component in existing urban SEB models (Grimmond *et al* 2011). The same situation can also be noticed in this study. The original model (Sim_1, see table S1) gives a RMSE of 52.65 W m^{-2} and an IOA as low as 0.52 during the entire period.

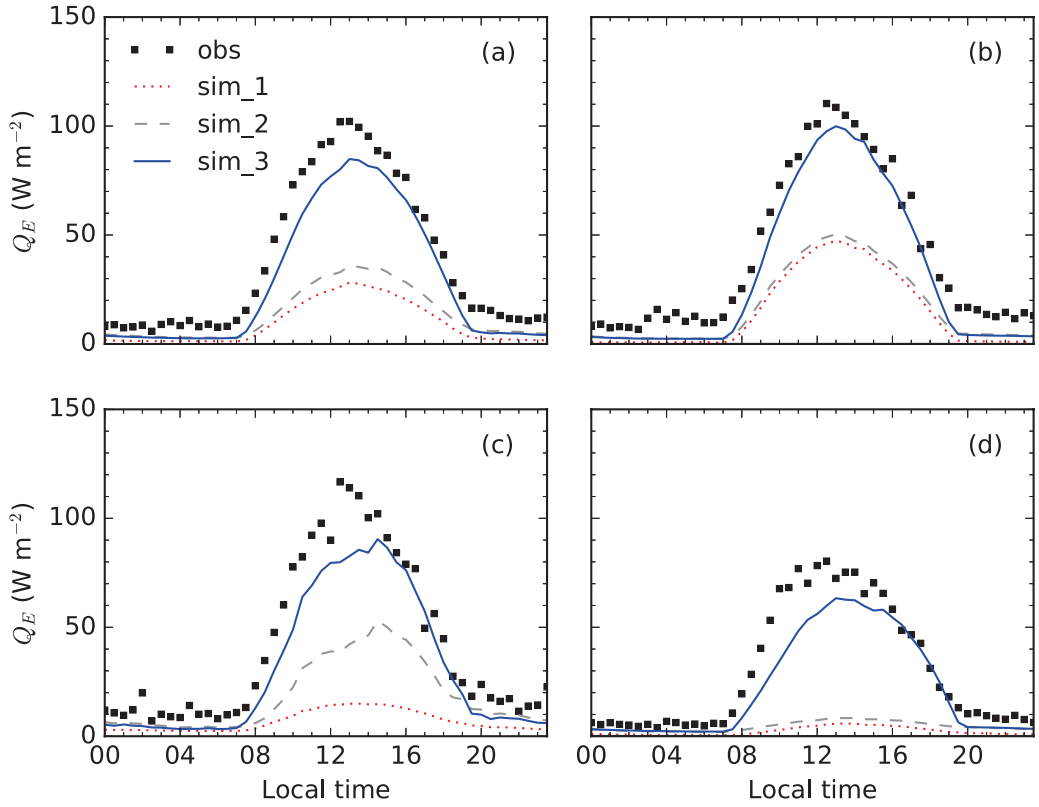

Figure 3. Same as figure 1 but for Q_E.

Incorporating urban hydrological processes into the coupled Noah/SLUCM model has achieved satisfactory results with improving modeling accuracy of Q_E in many cities such as Beijing, Phoenix and Montreal in previous studies (Miao and Chen 2014, Yang *et al* 2015). In our case, after considering hydrological processes in our study, though an increased average value of 12.68 W m^{-2} and a reduction of RMSE to 51.07 W m^{-2} are achieved during the entire period (Sim_2, see table S1), there is still a notable discrepancy between the modeled and observed Q_E. This situation may be explained by the different geography locations of the tropic city Singapore and mid-latitude cities. The mid-latitude cities are located in relatively dry areas with a high atmospheric demand and limited water available at the surface, whereas in Singapore the atmospheric demand is lower, while water in the urban fabric is more abundantly available.

In previous coupled Noah/SLUCM model simulations, the vegetation part of an urban site is generally represented by grassland without considering trees. In our case, the addition of tree evapotranspiration in Sim_3 sees a marked improvement in the accuracy of simulated Q_E. During the entire period, the RMSE and mean biased error (MBE) drop to 38.71 W m^{-2} and −11.99 W m^{-2}, respectively, and the IOA increases to 0.75 (table S1). From Sim_1 to Sim_3, the RMSEs reduces continuously (table S1), manifesting the improved model skills by including the tree evapotranspiration.

The model performance in predicting Q_E has a strong dependence on the seasonality. Sim_1 and Sim_2 give the poorest simulation results in the dry period, with the mean value of 2.54 W m^{-2} and 4.84 W m^{-2}, respectively, compared with the observed value of 34.39 W m^{-2} (table S1). Q_E is usually highly impacted by precipitation. Though there was only 2.2 mm precipitation during the dry period, the mean value of observed Q_E was still as high as 78% of that in other seasons (44.14 W m^{-2} in SW monsoon season, and 44.11 W m^{-2} in early NE monsoon season). There should be other processes contributing to Q_E during the dry period. One such process is the tree evapotranspiration, which has been demonstrated in Sim_3 (figure 3(*d*)). With added tree evapotranspiration, the RMSEs of Q_E decreases from 46.94 W m^{-2} (Sim_1) to 20.55 W m^{-2} (Sim_3), indicating that the systematic error has been greatly reduced and most of the discrepancy between the simulated and observed Q_E can be explained by random processes (e.g. due to uncertainties from input parameters). Another possible process is the urban irrigation. Although no regular urban irrigation is conducted in Singapore, in extremely dry period, it is reasonable to assume that some manual, sporadic irrigations may be carried out by local residents to mitigate the absence of water.

3.2.4. *Sensible heat flux* Q_H

The simulated Q_H exhibits a consistent performance during all seasons (figure 4). The RMSE of Q_H in Sim_1 is more than 35 W m^{-2}. With the added

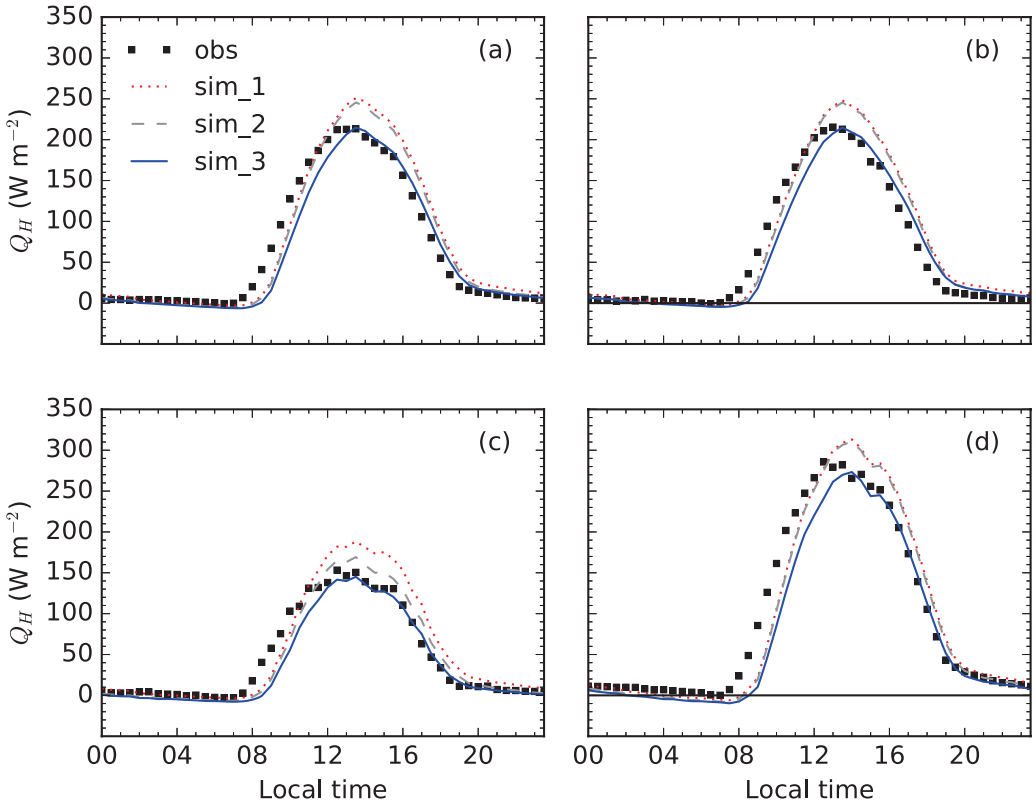

Figure 4. Same as figure 1 but for Q_H.

hydrological processes (Sim_2), the model performance improves accordingly. Nevertheless, Q_H is still overestimated until the tree effect is considered in Sim_3. The model shows notable improvement in Sim_3 in the early NE monsoon season (figure 4(*c*)), with RMSE reducing to 31.46 W m^{-2} from 34.87 W m^{-2} and 31.59 W m^{-2} in Sim_1 and Sim_2, respectively (table S1). The RMSEs and RMSEu also decrease with added hydrological processes and tree evapotranspiration (table S1).

A consistent lag in the simulated Q_H is found in all the seasons. Hysteresis starts from 0800 LT with peak value at 1300 to 1330 LT, slightly later than the observed peak at 1230 LT. This phenomenon is not typical as the long-term (2006–2013) average Q_H of Singapore peaks at 1300 LT, and 1400 LT for dry seasons (Roth *et al* 2017). The diurnal cycle of predicted Q_H corresponds more to the long-term statistics rather than the period under investigation here. Since the major goal of this study is to improve the prediction of Q_E, no efforts were made to fine tune the parameters related to Q_H. The observed lag in Q_H needs further investigation, but it is beyond the scope of the current study.

3.2.5. *Heat storage flux* Q_S

As both the simulated and observed ΔQ_S are calculated as the residual of the net radiation and the other energy components (see equation (2)), i.e. $(Q^* + Q_F) - (Q_H + Q_E)$, and no direct measurements are available for comparison, the modeling uncertainties of all other variables in equation (2) accumulate in ΔQ_S. The time shift resulting from Q_H leads to the time shift in ΔQ_S, and the negative and positive biases of Q^*, Q_H and Q_E offset each other. No appreciable difference between the three simulations can be observed, except a slight difference in Sim_3 near noon and sunset (1900 LT). The simulated results in all seasons show an overestimation before noon while underestimation during the second half of the day.

3.3. Further analysis of Q_E

3.3.1. *Taylor diagram*

Figure 6 shows normalized Taylor diagrams for Q^*, $L_\uparrow$, Q_H and Q_E for all simulations, observations and seasons. Observations are indicated by the star symbol at (1.0, 1.0, 0.0), correlation coefficients are plotted on polar axes, normalized standard deviations on *y*-axes and normalized RMSE are given by the inner grey circles.

The performance of Q^* shows no visible difference across all simulations, while the predicted $L_\uparrow$ is sensitive to the seasonality, with the best performance during the dry period and worst during the early NE monsoon season. The correlation coefficients of Q_H are in a narrow range from 0.9 to 0.95, with small variability in normalized standard deviation and normalized RMSE. A wide range of model performance is evident for Q_E. Correlation coefficients for all simulations are less than 0.7 except for Sim_3 during the dry period (indicated by the green circle symbol).

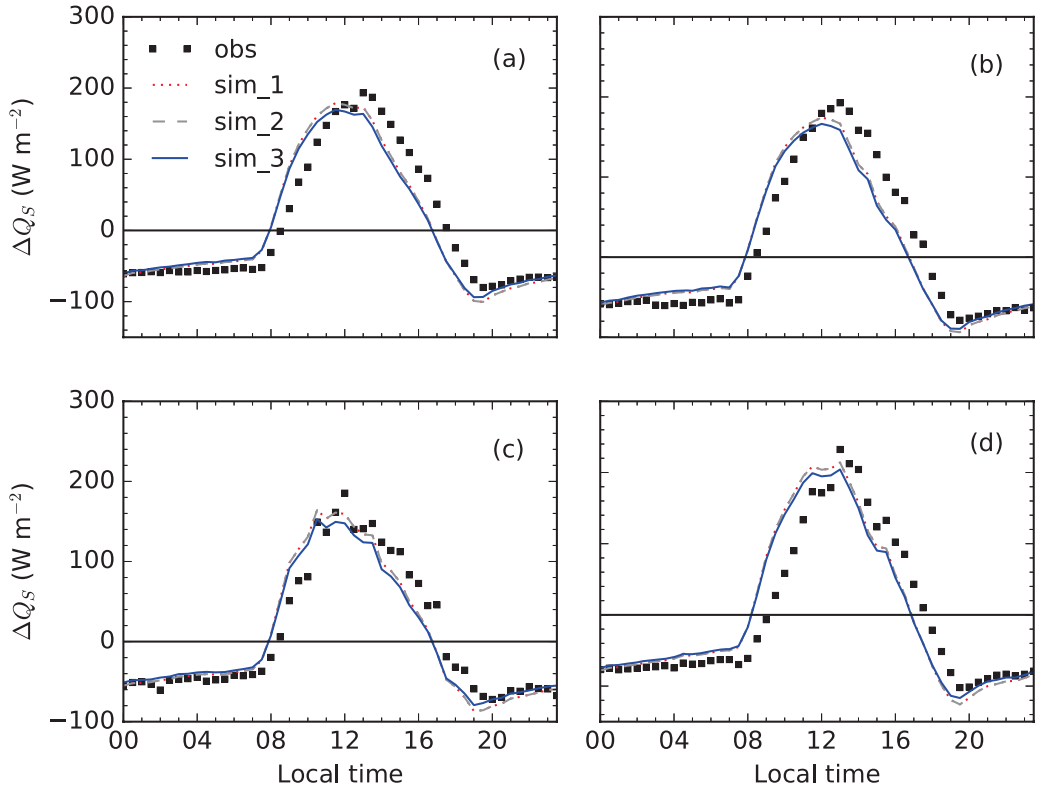

Figure 5. Same as figure 1 but for ΔQ_S.

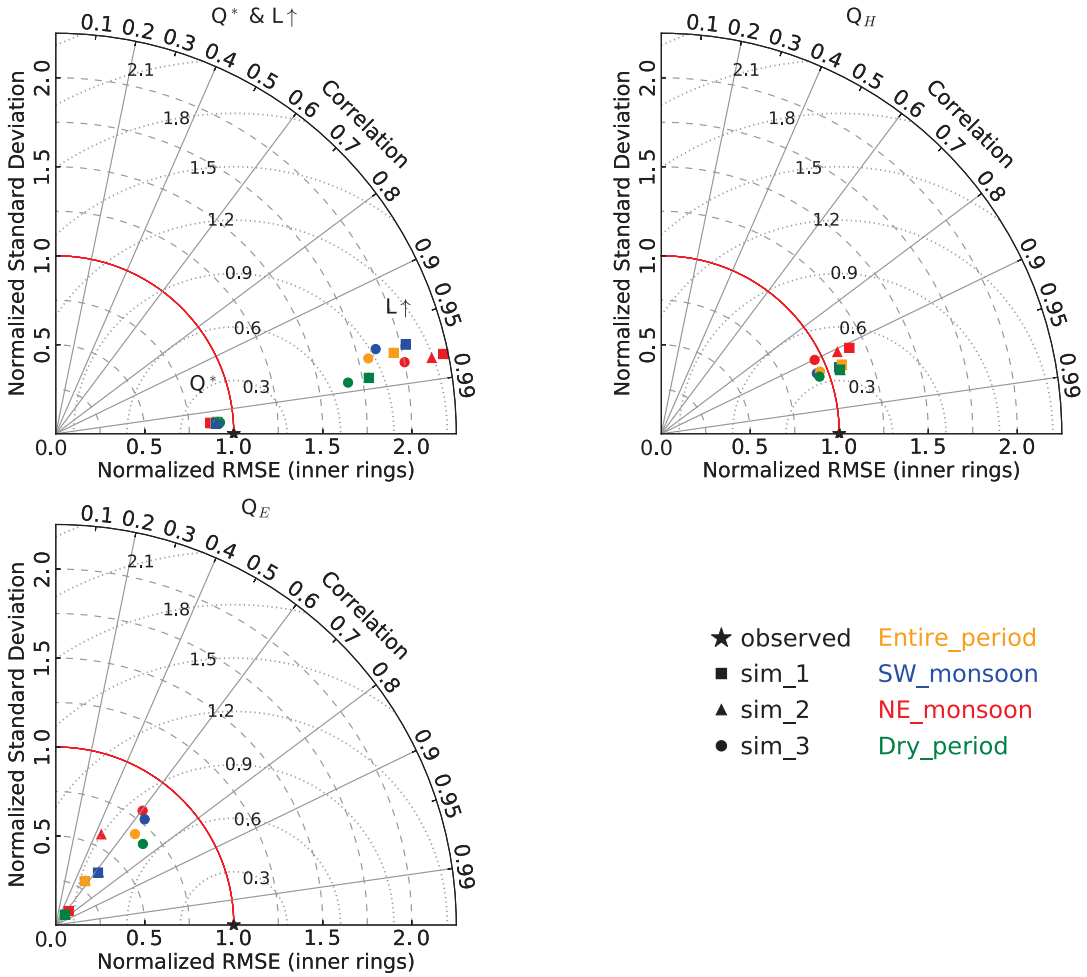

Figure 6. Normalized Taylor diagrams for Q^*, $L_\uparrow$, Q_H and Q_E for all simulations (symbols) and seasons (colors).

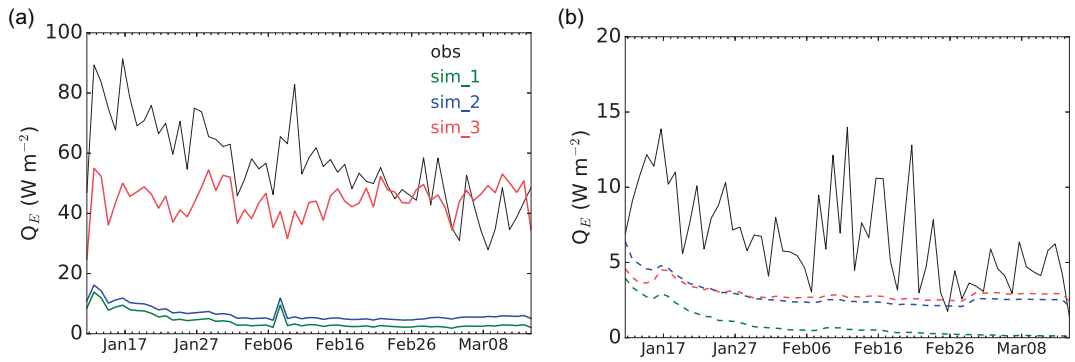

Figure 7. Daily averaged time series of observed and simulated Q_E for the (*a*) daytime and (*b*) nighttime during the dry period.

The normalized standard deviations are scattered from 0.0 to 0.8 and RMSE values are around 0.8 except for Sim_3 during the dry period (indicated by the green circle symbol, which is below 0.7). Overall, taking the tree evapotranspiration into account greatly improves the model performance in predicting Q_E. It can be seen from the diagram that the model with the tree evapotranspiration generally has the best performance during the dry period and early NE monsoon season with the new impervious evaporation scheme (indicated by the green and red circle symbols, respectively). During the dry period (green circle symbol), the simulated Q_E shows the highest correlation and lowest RMSE, while during early NE monsoon season (red circle symbol) the standard deviation of the simulated Q_E is the closest to the observational data.

3.3.2. *Model performance during dry period*

As revealed by the Taylor diagrams (figure 6), the Q_E simulation during the dry period with added tree evapotranspiration shows best performance. To examine Q_E simulation improvement during the dry period in detail, figure 7 compares the daily averaged Q_E from both observations and simulations during the daytime (figure 7(*a*)) and nighttime (figure 7(*b*)). An evident increase of all values is noted in Sim_3 during daytime with a magnitude 3 times larger than that in Sim_2, which suggests that urban tree evapotranspiration dominants the dry period's latent heat release. However, during nighttime, the model performance of Sim_3 is as bad as that of Sim_2, since no solar radiation is available for evapotranspiration at that time.

4. Conclusions and discussions

This study evaluated the performance of the coupled Noah/SLCUM model in a tropical suburban site during a 11 month period. Some urban hydrological processes (anthropogenic latent heat flux and evaporation from urban impervious surfaces) as well as the tree evapotranspiration were implemented in the model to improve the prediction skills of latent heat flux Q_E. Comparisons with the field measurements showed that the added hydrological processes can help improve the accuracy in predicting Q_E. However, there still remained much discrepancy between the simulated and observed Q_E until the tree evapotranspiration was included in the model. The inclusion of the tree evapotranspiration had been shown to greatly reduce the MBE and RMSE of simulated Q_E, particularly leading to much lower systematic RMSE, an indication of the improved prediction skills. During an unusual dry spell in early 2014 when there was little contribution from precipitation, the tree evapotranspiration was found to contribute most of Q_E. The improved model demonstrated little effect during nighttime, when the solar radiation needed for transpiration is missing. The results demonstrated that tree evapotranspiration plays a very important role in latent heat flux in an urban environment like Singapore, and ignoring the tree effect will result in underestimation of latent heat flux.

Similar studies in Vancouver, Canada (Krayenhoff *et al* 2014, Krayenhoff *et al* 2015) and Basel, Switzerland (Ryu *et al* 2016) have demonstrated the role of trees in improving latent heat flux prediction. It is therefore expected that the proposed improved model from the present study can be transferred to other tropical and temperate urban environments to produce improved latent heat flux prediction. For neighborhoods without the necessary observational data as input to the model (which is very common), the online simulation with the well-calibrated coupled WRF/UCM can be performed instead. The improved model can be applied to better predict a variety of important real-world issues facing urban dwellers, such as urban heat island mitigation, outdoor thermal comfort, building energy usage (when coupled with a building energy model), or water usage management during drought conditions (Vahmani and Ban-Weiss 2016).

Acknowledgments

This research is supported by the National Research Foundation Singapore (NRF) under its Campus for Research Excellence and Technological Enterprise

(CREATE) programme. The Center for Environmental Sensing and Modeling (CENSAM) is an interdisciplinary research group of the Singapore-MIT Alliance for Research and Technology (SMART). We thank Mr. YANG Jiachuan and Dr. WANG Zhihua at Arizona State University for providing the source code and their valuable suggestions.

ORCID iDS

Xian-Xiang Li https://orcid.org/0000-0002-8688-6206

References

Allen R G, Pereira L S, Raes D and Smith M 1998 Crop evapotranspiration-guidelines for computing crop water requirements-FAO Irrigation and drainage paper 56 *FAO, Rome*

Ballinas M and Barradas V L 2016 The urban tree as a tool to mitigate the urban heat island in Mexico city: a simple phenomenological model *J. Environ. Qual.* **45** 157–66

Best M J and Grimmond C S B 2015 Key conclusions of the first international urban land surface model comparison project *Bull. Am. Meteorol. Soc.* **96** 805–U18

Best M J and Grimmond C S B 2016 Modeling the partitioning of turbulent fluxes at urban sites with varying vegetation cover *J. Hydrol.* **17** 2537–53

Bosveld F and Bouten W 2001 Evaluation of transpiration models with observations over a douglas-fir forest *Agr. Forest Meteorol.* **108** 247–64

Chen F and Dudhia J 2001 Coupling an advanced land surface-hydrology model with the Penn State-NCAR MM5 modeling system. Part I: model implementation and sensitivity *Mon. Weather Rev.* **129** 569–85

Chen F *et al* 2011 The integrated WRF/urban modelling system: development, evaluation, and applications to urban environmental problems *Int. J. Climatol.* **31** 273–88

Chen F, Kusaka H, Tewari M, Bao J and Hirakuchi H 2004 Utilizing the coupled WRF/LSM/Urban modeling system with detailed urban classification to simulate the urban heat island phenomena over the Greater Houston area *5th Conf. on Urban Environment* (Vancouver, BC 23–27 August 2004) paper 9.11

Demuzere M, Harshan S, Jarvi L, Roth M, Grimmond C S B, Masson V, Oleson K W, Velasco E and Wouters H 2017 Impact of urban canopy models and external parameters on the modelled urban energy balance in a tropical city *Q. J. R. Meteorolog. Soc.* **143** 1581–96

Fernando H J 2012 *Handbook of Environmental Fluid Dynamics, Volume Two: Systems, Pollution, Modeling, and Measurements* (Boca Raton, FL: CRC Press)

Fong M and Ng L K 2012 *The Weather and Climate of Singapore* (Singapore: Meteorological Service)

Gentine P, Chhang A, Rigden A and Salvucci G 2016 Evaporation estimates using weather station data and boundary layer theory *Geophys. Res. Lett.* **43** 11661–70

Grimm N B, Faeth S H, Golubiewski N E, Redman C L, Wu J G, Bai X M and Briggs J M 2008 Global change and the ecology of cities *Science* **319** 756–60

Grimmond C, Blackett M, Best M, Baik J J, Belcher S, Beringer J, Bohnenstengel S, Calmet I, Chen F and Coutts A 2011 Initial results from phase 2 of the international urban energy balance model comparison *Int. J. Climatol.* **31** 244–72

Hagishima A, Narita K-I and Tanimoto J 2007 Field experiment on transpiration from isolated urban plants *Hydrol. Process.* **21** 1217–22

Harshan S, Roth M, Velasco E and Demuzere M 2017 Evaluation of an urban land surface scheme over a tropical suburban neighbourhood *Theor. Appl. Climatol.* (https://doi.org/10.1007/s00704-017-2221-7)

Kawai T and Kanda M 2010 Urban energy balance obtained from the comprehensive outdoor scale model experiment. Part I: basic features of the surface energy balance. *J. Appl. Meteorol. Climatol.* **49** 1341–59

Koster R 2015 'Efficiency space': a framework for evaluating joint evaporation and runoff behavior *Bull. Am. Meteorol. Soc.* **96** 393–6

Krayenhoff E, Christen A, Martilli A and Oke T 2014 A multi-layer radiation model for urban neighbourhoods with trees *Bound.-Layer Meteorol.* **151** 139–78

Krayenhoff E S, Santiago J L, Martilli A, Christen A and Oke T R 2015 Parametrization of drag and turbulence for urban neighbourhoods with trees *Bound.-Layer Meteorol.* **156** 157–89

Kusaka H, Kondo H, Kikegawa Y and Kimura F 2001 A simple single-layer urban canopy model for atmospheric models: comparison with multi-layer and slab models *Bound.-Layer Meteorol.* **101** 329–58

Lee S-H and Park S-U 2008 A vegetated urban canopy model for meteorological and environmental modelling *Bound.-Layer Meteorol.* **126** 73–102

Li X X, Koh T Y, Entekhabi D, Roth M, Panda J and Norford L K 2013 A multi-resolution ensemble study of a tropical urban environment and its interactions with the background regional atmosphere *J. Geophys. Res.-Atmos.* **118** 9804–18

Li X X, Koh T Y, Panda J and Norford L K 2016 Impact of urbanization patterns on the local climate of a tropical city, Singapore: an ensemble study *J. Geophys. Res.-Atmos.* **121** 4386–403

Loridan T, Grimmond C S B, Grossman-Clarke S, Chen F, Tewari M, Manning K, Martilli A, Kusaka H and Best M 2010 Trade-offs and responsiveness of the single-layer urban canopy parametrization in WRF: an offline evaluation using the MOSCEM optimization algorithm and field observations *Q. J. R. Meteorolog. Soc.* **136** 997–1019

Martilli A 2002 Numerical study of urban impact on boundary layer structure: sensitivity to wind speed, urban morphology, and rural soil moisture *J. Appl. Meteorol.* **41** 1247–66

McBride J L, Sahany S, Hassim M E, Nguyen C M, Lim S-Y, Rahmat R and Cheong W-K 2015 The 2014 record dry spell at Singapore: an Intertropical Convergence Zone (ITCZ) drought *Bull. Am. Meteorol. Soc.* **96** S126–30

Miao S and Chen F 2014 Enhanced modeling of latent heat flux from urban surfaces in the noah/single-layer urban canopy coupled model *Sci. China Earth Sci.* **57** 2408–16

Miao S, Chen F, Lemone M A, Tewari M, Li Q and Wang Y 2009 An observational and modeling study of characteristics of urban heat island and boundary layer structures in Beijing *J. Appl. Meteorol. Climatol.* **48** 484–501

Mitchell V G, Cleugh H A, Grimmond C S B and Xu J 2008 Linking urban water balance and energy balance models to analyse urban design options *Hydrol. Process.* **22** 2891–900

MSS 2014 *Annual Weather Review 2014* (Singapore: Meteorological Service and National Environmental Agency)

Oke T 1988 The urban energy balance *Prog. Phys. Geog.* **12** 471–508

Oke T R 1976 The distinction between canopy and boundary-layer urban heat islands *Atmosphere* **14** 268–77

Patz J A, Campbell-Lendrum D, Holloway T and Foley J A 2005 Impact of regional climate change on human health *Nature* **438** 310–7

Quah A K and Roth M 2012 Diurnal and weekly variation of anthropogenic heat emissions in a tropical city, Singapore *Atmos. Environ.* **46** 92–103

Ramamurthy P and Bou-Zeid E 2014 Contribution of impervious surfaces to urban evaporation *Water Resour. Res.* **50** 2889–902

Roth M 2000 Review of atmospheric turbulence over cities *Q. J. R. Meteorolog. Soc.* **126** 941–90

Roth M, Jansson C and Velasco E 2017 Multi-year energy balance and carbon dioxide fluxes over a residential neighbourhood in a tropical city *Int. J. Climatol.* **37** 2679–98

Ryu Y-H, Bou-Zeid E, Wang Z-H and Smith J A 2016 Realistic representation of trees in an urban canopy model *Bound.-Layer Meteorol.* **159** 193–220

Stewart I D and Oke T R 2012 Local climate zones for urban temperature studies *Bull. Am. Meteorol. Soc.* **93** 1879–900

Tan P Y and Sia A 2010 *Leaf Area Index of Tropical Plants: A Guidebook on its Use in the Calculation of Green Plot Ratio* (Singapore: Centre of Urban Greenery and Ecology)

Vahmani P and Ban-Weiss G 2016 Climatic consequences of adopting drought-tolerant vegetation over Los Angeles as a response to California drought *Geophys. Res. Lett.* **43** 8240–9

Velasco E, Roth M, Tan S, Quak M, Nabarro S and Norford L 2013 The role of vegetation in the CO_2 flux from a tropical urban neighbourhood *Atmos. Chem. Phys.* **13** 10185–202

Yang J, Wang Z-H, Chen F, Miao S, Tewari M, Voogt J A and Myint S 2015 Enhancing hydrologic modelling in the coupled weather research and forecasting–urban modelling system *Bound.-Layer Meteorol.* **155** 87–109

Yee A, Corlett R T, Liew S and Tan H T 2011 The vegetation of Singapore—an updated map *Gard. Bull. Singapore* **63** 205–12